Cell Tissue Res (2006) 326: 851–860
DOI 10.1007/s00441-006-0212-6

REGULAR ARTICLE

Yukiko Sato · Hiroyuki Kaneko · Sumiko Negishi · Ikuko Yazaki

Larval arm resorption proceeds concomitantly with programmed cell death during metamorphosis of the sea urchin *Hemicentrotus pulcherrimus*

Received: 22 August 2005 / Accepted: 29 March 2006 / Published online: 26 July 2006

Abstract Sea urchins are excellent models to elucidate metamorphic phenomena of echinoderms. However, little attention has been paid to the way that their organ resorption is accomplished by programmed cell death (PCD) and related cellular processes. We have used cytohistochemistry and transmission electron microscopy to study arm resorption in competent larvae of metamorphosing sea urchins, *Hemicentrotus pulcherrimus*, induced to metamorphose by L-glutamine treatment. The results show that: (1) columnar epithelial cells, which are constituents of the ciliary band, undergo PCD in an overlapping fashion with apoptosis and autophagic cell death; (2) squamous epithelial cells, which are distributed between the two arrays of the ciliary band, display a type of PCD distinct from that of columnar epithelial cells, i.e., a cytoplasmic type of non-lysosomal vacuolated cell death; (3) epithelial integrity is preserved even when PCD occurs in constituent cells of the epithelium; (4) secondary mesenchyme cells, probably blastocoelar cells, contribute to the elimination of dying epithelial cells; (5) nerve cells have a delayed initiation of PCD. Taken together, our data indicate that arm resorption in sea urchins proceeds concomitantly with various types of PCD followed by heterophagic elimination, but that epithelial organization is preserved during metamorphosis.

This investigation was supported in part by a Keio University special grant-in-aid for innovative collaborative research projects.

Y. Sato · H. Kaneko · S. Negishi
Department of Biology, Keio University,
Hiyoshi 4-1-1, Kohoku-ku,
Yokohama, 223-8521, Japan

Y. Sato (✉) · I. Yazaki
Department of Biology, Faculty of Science,
Tokyo Metropolitan University,
Minamiosawa 1-1, Hachioji,
Tokyo, 192-0397, Japan
e-mail: yukiko_s@center.tmu.ac.jp
Tel.: +81-426-771111 (3238)
Fax: +81-426-772559

Keywords Metamorphosis · Arm resorption · Programmed cell death · Epithelial cells · Mesenchyme cells · Nerve cells · Phagocytosis · Sea urchin, *Hemicentrotus pulcherrimus* (Echinodermata)

Introduction

Programmed cell death (PCD) contributes effectively to organ resorption in the developing body during metamorphosis of invertebrates and vertebrates. Some multiformity of PCD exists in its timing and manner in various types of cells and tissues constituting organs. For example, in anuran metamorphosis, apoptosis occurs in the spinal cord (Estabel et al. 2003) prior to apoptosis in the epithelia of the small intestine (Ishizuya-Oka 1996), in the fast muscle of the tail (Berry et al. 1998), and in the skin (Menon et al. 2000), all of which occur at approximately the same time. The tail nerve cord and the tail slow muscle, on the other hand, undergo a type of PCD that is distinct from apoptosis (Fox 1973; Elinson et al. 1999; Das et al. 2002). In certain types of metamorphosing insects, non-apoptotic PCD has also been reported in salivary glands (Bowen et al. 1993), labial glands (Zakeri et al. 1995), and some accessory planta retractor motoneurons (Kinch et al. 2003).

Transmission electron microscopy (TEM) provides details not only of subcellular events of PCD itself but also of heterophagic elimination in close cooperation with PCD. On the basis of TEM studies by Schweichel and Merker (1973) and many other investigators, Clarke (1990) has postulated that PCD should be classified into three categories. Apoptosis (type 1) is characterized by pyknosis of the nucleus accompanied by the condensation of chromatin into dense masses and the shrinkage of cell bodies with increased electron density of the cytoplasm. These events are followed by fragmentation of the cells into apoptotic bodies that are phagocytosed by other cells. In contrast, during autophagic cell death (type 2), numerous autophagic vacuoles are formed with single and multi-layered membranes. Pyknotic nuclei are un-

common in autophagic cells compared with those undergoing apoptosis. The cells shrink, and their cytoplasm increases in electron density. Heterophagic elimination occasionally occurs in autophagic cells. Non-lysosomal vesiculate cell death (type 3) on the other hand, has been further classified into non-lysosomal disintegration (type 3A) and cytoplasmic-type cell death (type 3B). Although both types 3A and 3B have in common that intracellular organelles become dilated during PCD, each type exhibits different terminal appearances. In type 3A, the cell membrane fragments exclusively into small pieces, whereas in type 3B, dilation of the organelles is followed by the production of considerable amounts of empty space in the cytoplasm. Cells undergoing type 3B PCD finally round up without any fragmentation and undergo heterophagic elimination.

The present study has aimed at characterizing arm resorption during the metamorphosis of sea urchins and at providing detailed information on PCD. In 1978, Chia and Burke (1978) reviewed various aspects of echinoderm metamorphosis and introduced the phenomenon of cell death as a topic; however, little consideration was given to PCD, because knowledge of PCD was not widespread at that time. No attempt has been made to understand the cellular processes of organ resorption in relation to PCD since then.

Yazaki and her colleagues (Yazaki and Harashima 1994; Yazaki 1995; Sato and Yazaki 1999) have shown that L-glutamine is an agent that induces metamorphosis synchronously among individual larvae in three species of sea urchins: *Pseudocentrotus depressus*, *Hemicentrotus pulcherrimus*, and *Anthocidaris crassispina*. This experimental system has the advantage of being easy to handle compared with other methods reported elsewhere (Burke 1983; Taniguchi et al. 1994; Yazaki 2002) and therefore seems to be useful for studying PCD and related cellular processes that occur during metamorphosis. When treated with L-glutamine, larvae of *A. crassispina* undergo metamorphosis with characteristic nuclear chromatin condensation in their epithelial cells during arm and oral hood resorption (Sato and Yazaki 1999). This observation suggests that apoptosis occurs during organ resorption in sea urchins (Sato 2003).

To elucidate PCD and related cellular processes that occur during arm resorption, we have used TUNEL and monodansyl cadaverine (MDC) labeling, immunohistochemistry, and electron microscopy on competent larvae of sea urchins *H. pulcherrimus* undergoing metamorphosis. Following treatment with L-glutamine, two kinds of epithelial cells (columnar and squamous) constituting the arm develop apoptosis attended by autophagic cell death and a cytoplasmic type of non-lysosomal vacuolated cell death, respectively. Secondary mesenchyme cells, probably blastocoelar cells, are revealed to eliminate the dying cells. This study further shows that the epithelium preserves its integrity during arm resorption and that nerve cells undergo PCD at a later time.

Materials and methods

Larval culture

Larvae competent for metamorphosis of *H. pulcherrimus* were obtained as described previously (Yazaki and Harashima 1994). Briefly, embryos at the prism stage were cultured at 17–20°C in sterilized natural sea water until the late eight-armed stages (7–8 weeks), under constant stirring with a paddle connected to a motor (30 rpm). They were fed *Chaetoceros gracilis* every day.

Induction of metamorphosis

Larvae were induced to metamorphose as described previously (Yazaki and Harashima 1994). Briefly, they were collected as a group of competent larvae for metamorphosis in plain artificial seawater (ASW; Jamarin U, Jamarin, Osaka, Japan), incubated in ASW containing 10^{-4} M L-glutamine (Nakaralai tesque, Kyoto, Japan; Gln-ASW) for 24 h, and replaced in plain ASW. Larvae treated with or without Gln-ASW are called Gln-ASW-treated or untreated larvae, respectively. The time course of metamorphosis was observed with a stereoscopic microscope (LEICA MZ APO; Leica, Tokyo, Japan).

Whole-mount TUNEL assay

Gln-ASW-treated and untreated larvae were fixed in ASW containing 4% paraformaldehyde for 20 min at room temperature and then washed three times with phosphate-buffered saline (PBS). They were examined by using the "In situ cell death detection kit, fluorescein" from Roche Diagnostics (Mannheim, Germany) following the manufacturer's instructions but with two modifications. First, the reaction mixture was diluted to a half concentration with the recommended buffer; second, all washing steps were carried out with PBS containing 0.1% Tween 20 (Wako Chemicals, Osaka, Japan; PBST). Specimens were examined by using an Olympus laser scanning confocal microscope (Fluoview FV 300; Olympus Optical, Tokyo, Japan). Images were processed by using Adobe Photoshop 6.0.

Propidium iodide staining of damaged cells

After treatment with Gln-ASW for 6 h, living Gln-ASW-treated larvae were incubated in ASW containing 10 μg/ml propidium iodide (PI; Wako Chemicals) and 10 μg/ml RNase A (Wako Chemicals) for 5 min in the dark at 20°C and then washed twice with ASW. In order to stop larvae swimming, their ciliary movements were inhibited by using a small amount of 100 mM sodium azide in ASW (Tamura et al. 1998). They were examined with an Olympus confocal laser scanning microscope.

Autophagic cell death detection

Autophagic vacuoles were assayed in vivo by the Biederbick method with slight modifications (Biederbick et al. 1995). Gln-ASW-treated and untreated larvae were incubated in ASW containing 0.1 mM MDC (Sigma-Aldrich, Mo., USA) for 20 min. After being rinsed three times with ASW, the ciliary movements of the swimming larvae were inhibited by ASW containing 100 mM sodium azide. MDC-labeled cells were viewed by using a fluorescence microscope IX71 (Olympus Optical). MDC emits green fluorescence when excited at 365 nm. All procedures were performed at room temperature.

Preparation of larvae for TEM

Gln-ASW-treated and untreated larvae were fixed with ASW containing 2.5% glutaraldehyde (Polyscience, Tokyo, Japan) and 1% osmium tetroxide (Polyscience) at room temperature for 1.5 h, washed three times with 90% ASW, dehydrated with a graded series of ethanol, and embedded in epoxy resin (Nisshin EM). Larval arms were sectioned (0.08 μm) by using a Porter-Blum MT2 ultramicrotome with a diamond knife. Sections were placed on EM fine-glide no. 100 grids (Nisshin EM, Tokyo, Japan), stained with 4% uranium acetate for 20 min and then with 0.4% lead citrate for 10 min, and viewed by using a JEOL 1001 electron microscope (Hitachi, Tokyo, Japan) at 80 kV.

Immunohistochemistry combined with TUNEL assay

Some Gln-ASW-treated larvae that had been used for the TUNEL assay were also subjected to immunofluorescence staining. The larvae were incubated with conditioned medium from a 1E11 hybridoma culture (Nakajima et al. 2004) for 30 min at room temperature, washed three times with PBST, incubated further for 15 min with Alexa-TM-546 goat anti-mouse IgG (H+L) conjugate (highly cross-adsorbed) diluted to 1/200 in PBS supplemented with 10% fetal bovine serum (Invitrogen, Calif., USA), washed with PBST, and examined by using an Olympus laser scanning confocal microscope.

Results

Larval arm resorption during metamorphosis induced by L-glutamine

Metamorphosis proceeded with high reproducibility in larvae of *H. pulcherrimus* treated with Gln-ASW for 24 h and subsequently incubated in plain ASW for 48 h. The larvae revealed dynamic resorption of parts of their bodies and eversion of the echinus rudiment (Fig. 1). On further rearing, they completed their metamorphosis, growing into feeding juveniles (not shown). When the Gln-ASW treatment was prolonged for 48 h, the larvae failed to metamorphose. These observations were comparable to those reported previously (Yazaki 1995).

Figure 1 also shows the detailed dynamics of arm resorption. Within 6 h after the start of Gln-ASW treatment, some arms began to shorten, while others remained intact with respect to their length (Fig. 1b). At 24 h, when the larvae were transferred from Gln-ASW to incubation in plain ASW, all of the arms had shortened by different proportions (Fig. 1c). After 48 h of incubation in plain ASW, most arms had been resorbed into the juvenile body, whereas the remaining arms continued to shorten (Fig. 1d). Thus, asynchronous arm resorption occurred during metamorphosis induced by treatment with Gln-ASW. Hereafter, we refer to the proportion of arm resorption as the percentage of shortening shown by each arm.

Cytohistochemical signals for apoptosis and autophagic cell death during arm resorption

To identify apoptosis during arm resorption, the Gln-ASW-treated and untreated larvae with various proportions of arm resorption were processed for the whole-mount TUNEL

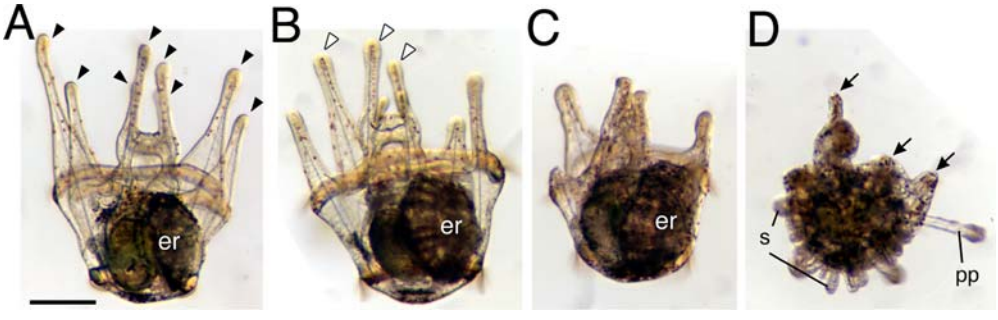

Fig. 1 Metamorphosis and arm resorption of *H. pulcherrimus*. **a** A larva competent for metamorphosis, just before treatment with Gln-ASW (Gln-ASW-untreated larva). The eight arms (*arrowheads*) and echinus rudiment (*er*) have fully developed. **b** After a 6-h Gln-ASW treatment, three arms (*white arrowheads*) have not shortened as yet and are referred to as 0% resorption in this study. The other arms have begun to resorb. **c** After a 24-h Gln-ASW treatment, all arms reveal 30%–50% resorption. **d** By 48 h after the Gln-ASW treatment, the echinus rudiment everts, resulting in the appearance of primary podia (*pp*) and spines (*s*) from the larval body. Some arms reveal 70% resorption (*arrows*), whereas others have completely resorbed. *Bar* 200 μm

labeling assay. This assay showed a small number of apoptotic cells in the arms of Gln-ASW-untreated larvae (Fig. 2a,b). Positive TUNEL signals were scattered over the arms of Gln-ASW-treated larvae in 0% resorption, although the arms had not yet started to shorten (Fig. 2c,d), and remained in arms with various proportions of resorption (30%–70% resorption; Fig. 2e,f). Since positive signals of TUNEL labeling were occasionally obtained from necrotic cell death rather than apoptosis (Seipp et al. 2001), the Gln-ASW-treated larvae were subjected to live PI-staining, which showed few cells in 0% resorption (Fig. 2g,h), indicating that treatment with Gln-ASW induced the larvae to undergo apoptosis, but not necrotic cell death.

The MDC method was performed both in Gln-ASW-treated and in untreated larvae to identify autophagic vacuoles, a hallmark of autophagic cell death. In contrast to the Gln-ASW-untreated larvae (Fig. 3a,b), MDC-positive signals were discernable in arms undergoing resorption (Fig. 3c,d; 30% resorption). There was no difference in the appearance of positive signals among the arms revealing various proportions of resorption (not shown). Determination of whether the MDC-positive signals overlapped with the TUNEL-positive signals was not possible.

TEM analysis of PCD during arm resorption

Gln-ASW-untreated larvae

Figure 4a shows a cross section and a representation of arms of Gln-ASW-untreated larvae; columnar and squamous epithelial cells are the main cellular constituents of the epithelia, which also have an outer and inner extracellular matrix (ECM), viz., the hyaline and basal lamina (Fig. 4). The columnar epithelial cells form two arrays of ciliary bands. Squamous epithelial cells located in the aboral and the oral areas are also demarcated by rows of ciliary bands. In the aboral area of epithelia, the pigment cells are distributed among the squamous epithelial cells (Fig. 4a). The bulk of nerve fibers are buried in the basal part of the ciliary bands, and some nerve fibers are oriented underneath the squamous epithelial cells (not shown). The primary mesenchyme cells are located in the middle area of the blastocoel, which is delimited from the epithelia by the basal lamina. Part of the cytoplasm of the primary mesenchyme cells lies around the spicule (Fig. 4a).

None of the cells reveal morphological features of PCD as shown in the ongoing stage of arm resorption. The nuclear material of the two types of epithelial cells in the arms is homogeneous, although that of the columnar epithelial cells stains slightly more densely than that of the squamous epithelial cells (Fig. 4b,c). Each of the cell types is also filled with developed cytoplasm (Fig. 4b,c), and the mitochondria not dilated (cf. Fig. 5f). Phagocytic figures are not discernible in either type of cell.

Stage of 0% resorption in Gln-ASW-treated larvae

Morphological alterations were observed in both columnar and squamous types of epithelial cells in Gln-ASW-treated larvae, even though arm resorption had not yet been initiated (Fig. 5). In the columnar epithelial cells, the chromosomes of the nuclei became condensed, a morphological signs of apoptosis (Fig. 5a; cf. Fig. 4b). These cells also developed numerous autophagic vacuoles, the hallmark of autophagic

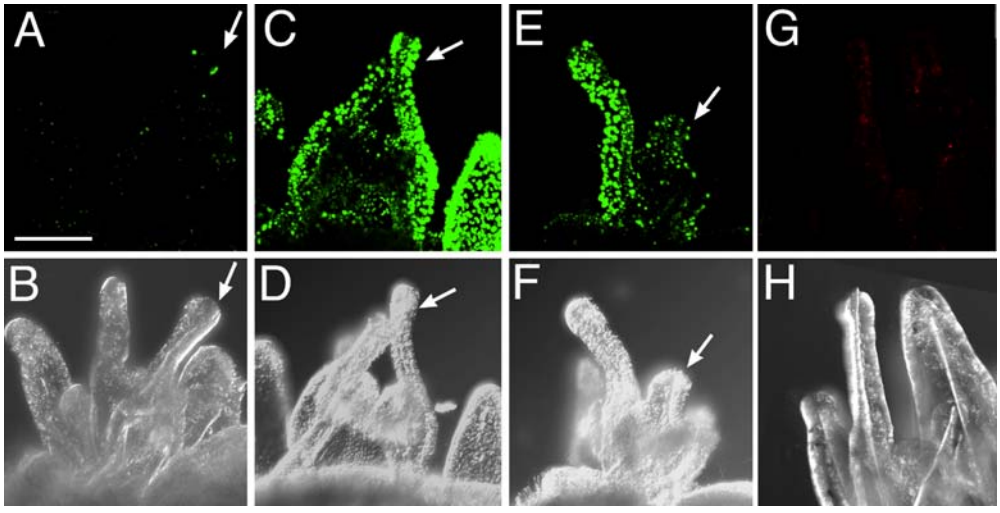

Fig. 2 Detection of apoptosis and necrotic cell death during Gln-ASW-induced arm resorption. Paired microphotographs of arms by fluorescence (**a**, **c**, **e**, **g**) and interference (**b**, **d**, **f**, **h**) microscopy. TUNEL assay (**a**–**f**) and propidium iodide staining (**g**, **h**) were used on different larvae (*arrows* same arms in **a** and **b**, **c** and **d**, and **e** and **f** by different microscopic methods and correspondence with one another in **a**–**f**). **a**, **b** Arms of Gln-ASW-untreated larvae. **c**, **d** Arms revealing 0% resorption (6-h Gln-ASW treatment). **e**, **f** Arms revealing 50% resorption (24-h Gln-ASW treatment). The apoptotic signals (*green*) increase in numbers in the arms after the onset of Gln-ASW treatment. **g**, **h** Arms revealing 0% resorption (6-h Gln-ASW treatment). A few dying cells (*red*) are seen in the larval arms. The fluorescent microphotographs are stacked images consisting of 46 (**a**), 40 (**c**), 51 (**e**), and 44 (**g**) optical sections. *Bar* 100 μm

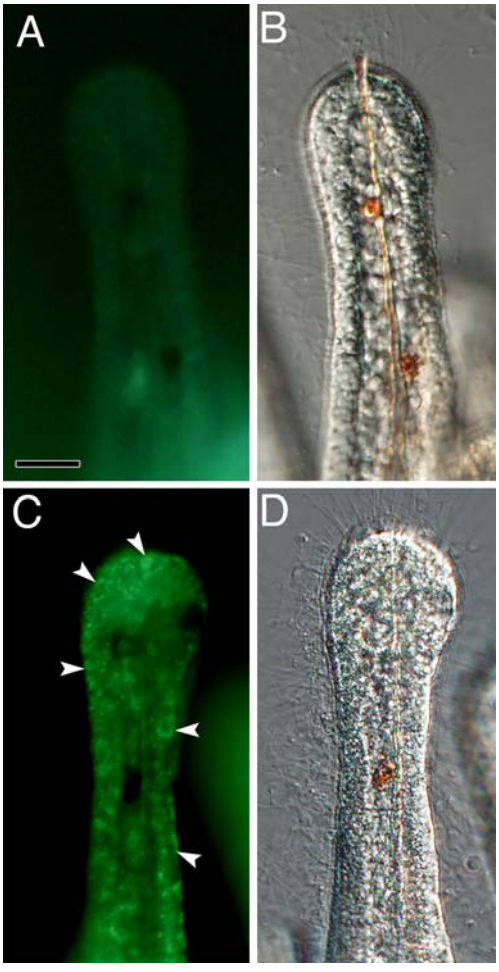

Fig. 3 Detection of autophagic vacuoles during Gln-ASW-induced arm resorption. The MDC method was used on Gln-ASW-treated (**c**, **d**) and untreated (**a**, **b**) larvae to identify autophagic cell death by the numerous autophagic vacuoles. Microphotographs were taken as overlapping images of fluorescence (**a**, **c**) and interference microscopy (**b**, **d**). Signals from autophagic vacuoles (*arrowheads*) were significantly increased in number during 30% resorption (**c**). *Bar* 100 μm

cell death (Fig. 5b,c). Such autophagic vacuoles included cytoplasmic material: some were partially encapsulated by membranes (Fig. 5b, arrowhead), whereas others were completely enclosed (Fig. 5c, arrowheads). The mitochondria were slightly dilated (not shown). The squamous epithelial cells revealed contorted nuclei, from which the nuclear material had been emptied (Fig. 5d, cf. Fig. 4c). The majority of mitochondria were considerably more dilated (Fig. 5e, arrowheads) compared with those of the Gln-ASW-untreated larvae (Fig. 5f, arrowheads).

Stage of 30%–50% resorption in Gln-ASW-treated larvae

Some columnar epithelial cells entered the advanced phase of apoptosis and autophagic cell death. Clumps of chromatin and fragmented forms of nuclei were readily visible (Fig. 6a, arrowheads). Some autophagic vacuoles appeared to have developed into clear vesicles (Fig. 6c, arrowheads) via autolysosomes (Fig. 6b, arrowheads). Compared with Fig. 5c, a considerable decrease in the amount of cytoplasmic material was observed in the autophagic vacuoles (Fig. 6b,c). The majority of squamous epithelial cells had empty spaces in their nuclei and cytoplasm (Fig. 6d). In such cells, intracellular organelles could no longer be detected, although both the plasma membrane and cell-to-cell junctions were preserved (Fig. 6e).

Secondary mesenchyme cells were frequently observed in the blastocoel. They were morphologically distinct from the primary mesenchyme cells and revealed considerable development of pseudopodia (Fig. 6d; see also Discussion). Some of them extended their pseudopodia across the basal lamina and into the region in which the squamous epithelial cells were distributed (Fig. 6d, arrow). Such penetration was limited to areas of squamous epithelial cells, but not of columnar epithelial cells. These secondary mesenchyme cells developed phagosomes in which cell debris was included (Fig. 6d,f).

Stage of 70% resorption in Gln-ASW-treated larvae

Columnar epithelial cells occupied the arm at a higher density than other cell types (Fig. 7a). Some columnar cells had shrunk; they appeared to be abnormally dark, and their nuclear chromatin was completely clumped (Fig. 7b, arrow). They did not show any intracellular organelles or adhesive structures with neighboring cells and included increased numbers of clear vesicles (Fig. 7b, arrow). We termed this phenotype as an “apoptotic-body-like” structure. Other columnar epithelial cells had further degenerated in the epithelia and in the blastocoelic space (Fig. 7b). Closer observation revealed that such degenerations were engulfed by secondary mesenchyme cells. The cytoplasm of such cells appeared much enlarged (Fig. 7b, see also Fig. 7c). The basal lamina was difficult to discern at this location (Fig. 7b).

Cell adhesion sites were seen between columnar epithelial cells that had not entered the terminal phase of PCD (Fig. 7d); the tandem structure of septate desmosomes was present among their intricate pseudopodia (Fig. 7d, arrowheads), and the hyaline layer was associated with no underlying disorganization (Fig. 7a; see also Figs. 5a,d, 6d).

Delayed PCD occurs in nerve cells

Entire nerve cells are difficult to observe by TEM. Figure 8 shows a rare micrograph of a nerve cell in a Gln-ASW-treated larvae. In this sample (30%–50% resorption), neither severe condensation of nuclear chromatin nor cytoplasmic degeneration can be discerned. This observation suggests that nerve cells may undergo delayed PCD in the epithelia.

To examine this hypothesis, a double-staining experiment in which the TUNEL method was combined with

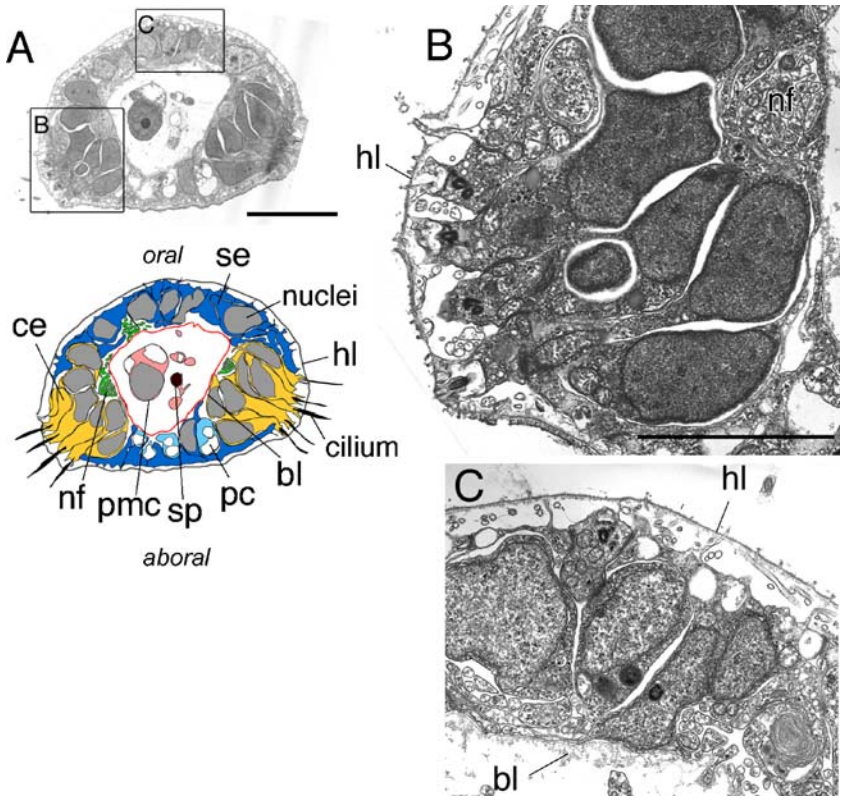

Fig. 4 Cellular and extracellular matrix (ECM) components in the arms of Gln-ASW-untreated larvae. **a** Electron micrograph of a cross section of the arm (*top*) and a representation of this section (*bottom*; *ce* columnar epithelial cells, *se* squamous epithelial cells, *hl* hyaline layer or outer ECM, *bl* basal lamina or inner ECM, *pc* pigment cells, *sp* spicule, *pmc* primary mesenchyme cells, *nf* nerve fibers). **b** Higher magnification of *rectangle B* in **a**. Columnar epithelial cells (*hl* hyaline layer, *nf* nerve fibers). **c** Higher magnification of *rectangle C* in **a**. Squamous epithelial cells (*hl* hyaline layer, *bl* basal lamina). *Bars* 10 μm (**a**), 5 μm (**b**, **c**)

immunolabeling by using a nerve cell marker was conducted in fixed specimens from the various stages of arm resorption shown by Gln-ASW-treated larvae. No apoptotic signals overlapped with nerve cells at 0% arm resorption (Fig. 9a–c). In several trials, coinciding images were first detected in a few nerve cells of arms revealing 50% resorption (Fig. 9d–f). The nerve fibers were oriented without any disrupted forms in the epithelia (Fig. 9b,e).

Discussion

We have shown, in this study, that PCD is an important component of larval arm resorption during the metamorphosis of *H. pulcherrimus*. When competent larvae are treated with Gln-ASW, many TUNEL- and MDC-positive signals extend over the arms (Figs. 2, 3). Our results indicate that the constituent cells of arms undergo at least two types of PCD: apoptosis and autophagic cell death. This hypothesis is supported by the PI-staining studies (Fig. 3g,h). Moreover, TEM observations have clarified the precise aspects of PCD and its related cellular processes in the arms of larval *H. pulcherrimus*. We summarize five critical findings below.

The first and second findings pertain to the category of PCD shown by the two kinds of epithelial cells. In columnar epithelial cells, two distinct types of PCD (apoptosis and autophagic cell death) occur simultaneously in individual cells. This notion is supported by the presence of apoptotic-body-like structures, in which dense clumps of chromatin and clear vesicles derived from autophagic vacuoles are prominent (Fig. 7b). Each of those two structures is characteristic of apoptosis and autophagic cell death, respectively. The cytohistochemical signals of the the TUNEL and MDC detection methods seem to overlap in columnar epithelial cells (Figs. 2, 3). Similar ultrastructural features have been noted in prothoracic gland resorption during the metamorphosis of *Manduca sexta* (Dai and Gilbert 1997) and in MF7 cells in culture (Zakeri et al. 1995). In the squamous epithelial cells of the larval arms, on the other hand, death is characterized by contorted nuclear morphology, dilation of organelles, and a marked emptiness of the nucleus and cytoplasm (Fig. 6d). These features resemble the cytoplasmic type of non-lysosomal vacuolated cell death (type 3B) as mentioned in the Introduction. The squamous epithelial cells do not have broken cell membranes and do not round up (Fig. 6d). The type of PCD occurring in these cells might therefore be a variant of type 3 PCD or an unknown type of PCD. Thus, two distinct types of PCD occur in epithelial cells during the process of arm resorption. The type of PCD that occurs in the pigment cells, which are also constituent cells of the epithelia (Fig. 4), remains unclear. We have not examined the type of PCD that occurs in the primary mesenchyme cells, which are known to play a role in spiculogenesis, by TEM. Preliminary experiments with TUNEL staining and specific immunofluorescent markers (SM30 and SM50, kindly supplied by Dr. Kitajima) have revealed that apoptosis occurs at least in some of these cells.

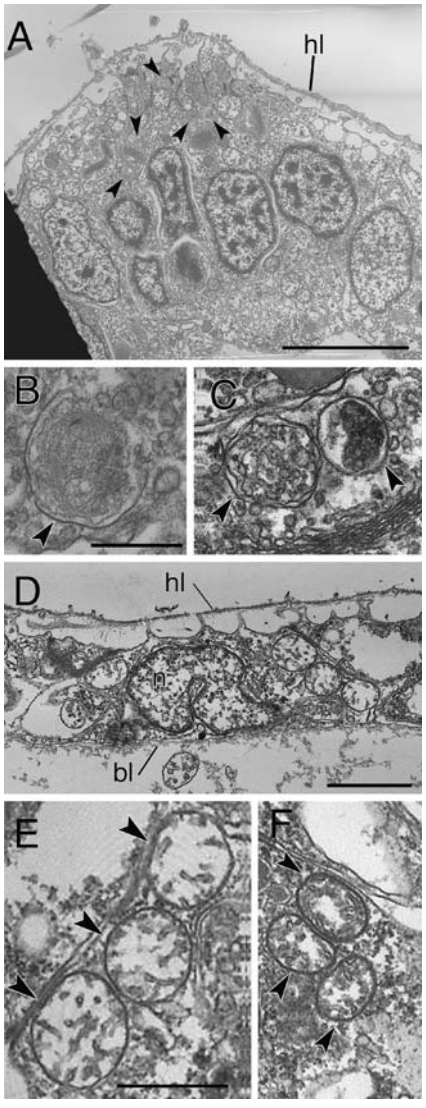

Fig. 5 Electron micrographs of an arm of a Gln-ASW-treated larva (0% resorption). **a** Columnar epithelial cells (*hl* hyaline layer). All eight nuclei have initiated chromosome condensation (*arrowheads* autophagic vacuoles). **b**, **c** Higher magnifications of autophagic vacuoles. The autophagic vacuole shown in **b** seems to be at an earlier phase than that in **c**, because the cytoplasmic material in **b** is not completely surrounded by the membranous structure (*arrowheads*). **d** Squamous epithelial cell (*hl* hyaline layer, *bl* basal lamina). **e**, **f** Mitochondria of squamous epithelial cells seen in Gln-ASW-treated (**e**) and untreated larvae (**f**). Mitochondria in **e** are considerably more dilated than those in **f** (*arrowheads*). *Bars* 5 μm (**a**), 0.5 μm (**b**, **c**), 2 μm (**d**), 1 μm (**e**, **f**)

Third, the integrity of the epithelia is preserved by adhesion among its constituent cells and the structural architecture of the ECM throughout the arm resorption process. Indeed, columnar epithelial cells retain septate desmosomes, one type of junctional complex, until the cells are transformed into an apoptotic-body-like structure (Fig. 7c). Septate desmosomes also remain between squamous epithelial cells, even when their cytoplasm has been lost (Fig. 6d,e). The hyaline layer, which is the outer ECM of the epithelium, is maintained intact until at least a late stage of arm resorption (70% resorption), although the basal lamina disappears locally (Fig. 7c). These observations include the differences in the time taken for cells to undergo PCD. This is also the case with the asynchronous PCD in columnar epithelial cells: a subgroup of them enters the terminal phase of PCD, while others initiate PCD (Fig. 7a). Such relationships between the integrity of the epithelium and PCD are rare. Evidence has accumulated in *Drosophila melanogaster* that PCD occurs concomitantly with the loss of cell adhesion during the formation of new organs during metamorphosis (Araujo et al. 2003; Hiesinger et al. 1999).

The fourth finding concerns the heterophagic elimination of dying cells. As arm resorption proceeds, the secondary mesenchyme cells are observed not only to extend their pseudopodia into epithelia in which squamous epithelial cells are undergoing PCD (Fig. 6d), but also to include cell debris within their phagolysosomes (Fig. 6f). In addition, the secondary mesenchyme cells phagocytose the numerous apoptotic-body-like structures derived from columnar epithelial cells both in the epithelia and blastocoelic regions (Fig. 7b). Secondary mesenchyme cells are categorized into pigment cells, muscle cells, coelomic pouch cells, and blastocoelar cells (Cameron et al. 1991). The cell type shown in this study to be involved in heterophagic elimination is probably the blastocoelar cell, which develops filopodia in the blastocoel (Tamboline and Burke 1992). The ability of blastocoelar cells to phagocytose foreign bodies (Silva 2000; Silva 2002) might provide a way of scavenging the dying cells. Phagocytic cells are known to display syncytium formation during the scavenging process in a wide variety of animals (Metchnikoff 1968; Papadimitriou and Walters 1979; Pavans de Ceccatty 1982; Dan-Sohkawa et al. 1993). The abundant cytoplasm seen in Fig. 7b might be caused by the fusion of blastocoelar cells with each other to phagocytose the dying cells as they accumulate in the blastocoel. Blastocoelar mesenchyme cells are probably activated to eliminate the dying cells without themselves undergoing PCD during metamorphosis.

Lastly, we should mentioned that nerve cells undergo PCD at a later time point. This has been deduced from the following observations: the nucleus and cytoplasm of nerve cells show little decay (Fig. 8), and TUNEL-positive signals are not apparent in nerve cells, even when PCD occurs in the columnar and squamous epithelial cells (Fig. 9). These findings strengthen the hypothesis that different cell types initiate PCD at different times during arm resorption in metamorphosis. In other sea urchin species, nerve cells have been shown to induce metamorphosis, including arm resorption, upon an electrical stimulus to the oral ganglions (Burke 1983). Nerve cells are also reported to be interconnected between the arms and oral hood (Beer et al. 2001). Whether nerve cells play some regulatory role(s) in the commitment of columnar and squamous epithelial cells to undergo PCD in *H. pulcherrimus* remains to be determined.

We conclude that columnar and squamous epithelial cells undergo distinct types of PCD to preserve epithelial integrity throughout arm resorption during the metamor-

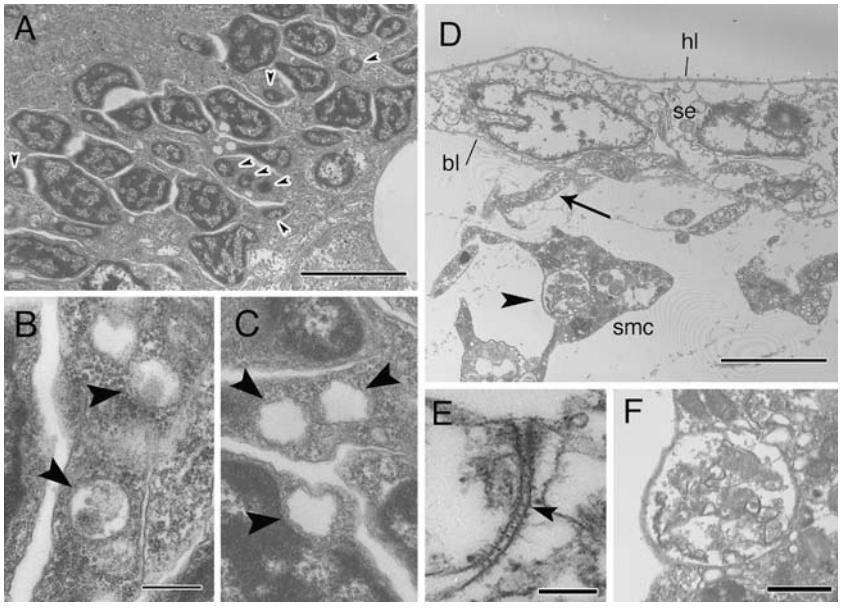

Fig. 6 Electron micrographs of an arm of a Gln-ASW-treated larvae (30%–50% resorption). **a** Columnar epithelial cells (*arrowheads* fragmented nuclei). **b**, **c** High magnification of two advanced forms of autophagic vacuoles. Note that the cytoplasmic material is considerably digested (*arrowheads*). **d** Empty squamous epithelial cells (*se*) and secondary mesenchyme (*smc*). The mesenchyme cell extends a pseudopodium (*arrow*) across the basal lamina (*bl*) into the squamous epithelial cell layer (*arrowhead* phagocytic vacuole of the mesenchyme cell, *hl* hyaline layer). **e** Septate desmosome. The characteristic tandem structure is seen between squamous epithelial cells that have lost their cytoplasmic materials. **f** Higher magnification of **d**. Cell debris is included in the phagocytic vacuole. *Bars* 5 μm (**a**, **d**), 0.5 μm (**b**, **c**), 0.2 μm (**e**), 1 μm (**f**)

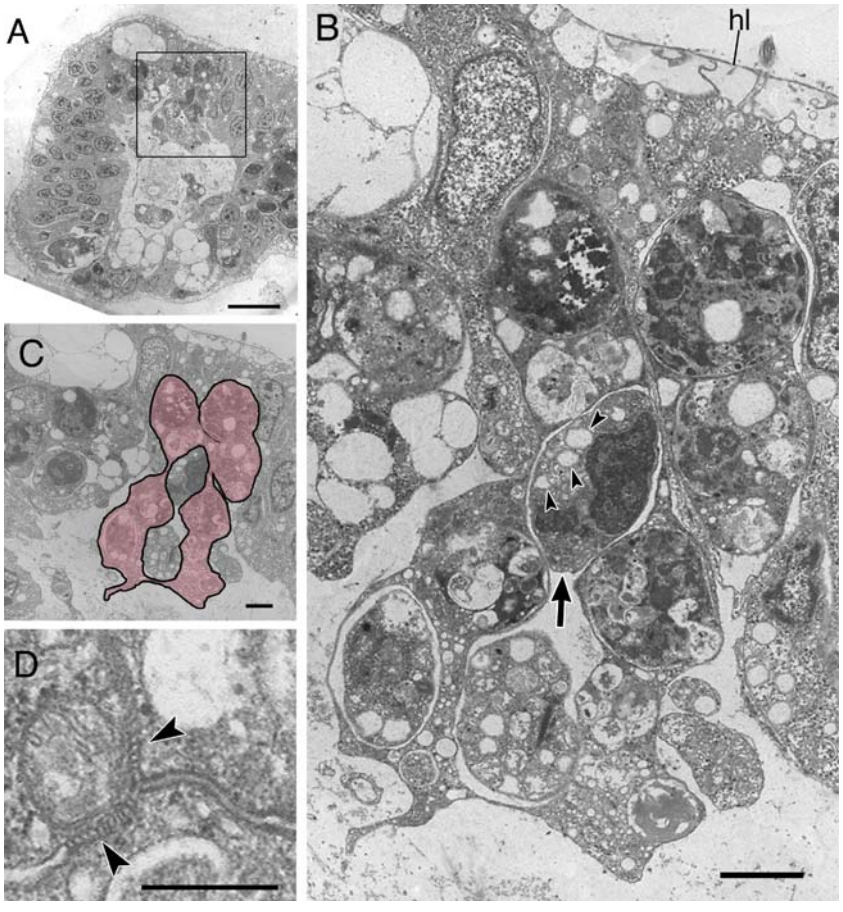

Fig. 7 Electron micrographs of an arm of a Gln-ASW-treated larva (70% resorption). **a** Low-power image of an arm mostly occupied by columnar epithelial cells (*rectangle* shown at higher magnifications in **b**, **c**). **b** Several columnar epithelial cells are phagocytosed by secondary mesenchyme, resulting in degeneration (*hl* hyaline layer). Note that the apoptotic-body-like structure (*arrow*) contains condensed and fragmented forms of nuclei and clear vesicles (*arrowheads*). It has not yet been phagocytosed by the mesenchyme cell. **c** The expanded cytoplasm of the mesenchyme cell is in *pink* (cf. **b**). **d** Septate desmosome (*arrowheads*) between columnar epithelial cells. This junctional complex is seen between cells that have not advanced into the phase of apoptotic-body-like structures. *Bar* 10 μm (**a**), 2 μm (**b**, **c**), 500 nm (**d**)

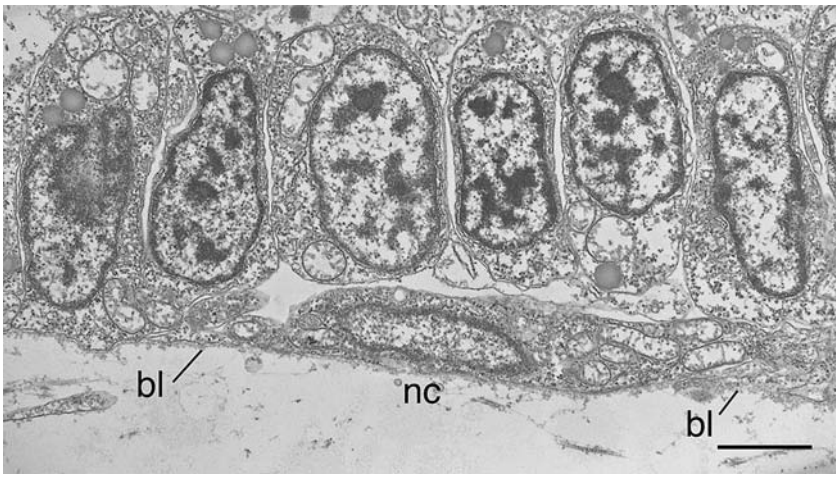

Fig. 8 Electron micrograph of a nerve cell (*nc*) in Gln-ASW-treated larva (30% resorption). No morphological signs of PCD are seen in the nerve cell. Note that the columnar epithelial cells have entered PCD. The morphological features of these cells resemble those shown in Fig. 5a (*bl* basal lamina). *Bar* 5 μm

phosis of sea urchins. Heterophagic elimination by blastocoelar cells, one member in the secondary mesenchyme cell group, also occurs to remove dying cells. Moreover, nerve cells undergo PCD at a later time. These findings indicate that, in sea urchins, not only does arm resorption proceed in a fashion reminiscent of PCD in other animals, but also an interesting multiformity exists, especially in the types and timing of initiation of PCD. Therefore, the phenomenon of arm resorption in sea urchins provides us with an excellent experimental system to clarify the mechanisms underlying organ resorption during metamorphosis. Future work will focus on two interesting questions that have arisen from this study: (1) how do nerve cells regulate the PCD occurring in epithelial cells, and (2) how do blastocoelar mesenchyme cells recognize epithelial cells undergoing PCD?

Acknowledgements We are grateful to Prof. Yoshinori Ohsumi and Dr. Eiko Oita for their kind suggestions regarding the identification of the morphology of autophagic vacuoles, to Profs. Kiyoaki Kuwasawa and Shinichi Hisanaga for their valuable discussions, and to Dr. Isao Uemura for his technical advice on electron microscopy. We are indebted to members of the Marine and Coastal Research Center of Ochanomizu University and to Profs. Takashi Suyemitsu and Masato Kiyomoto, Ms. Mamiko Yajima and Ms. Ayumi Kikuchi for supplying sea urchin larvae. Our thanks are also due to Dr. Masashi Noguchi for his useful suggestions and for supplying larvae.

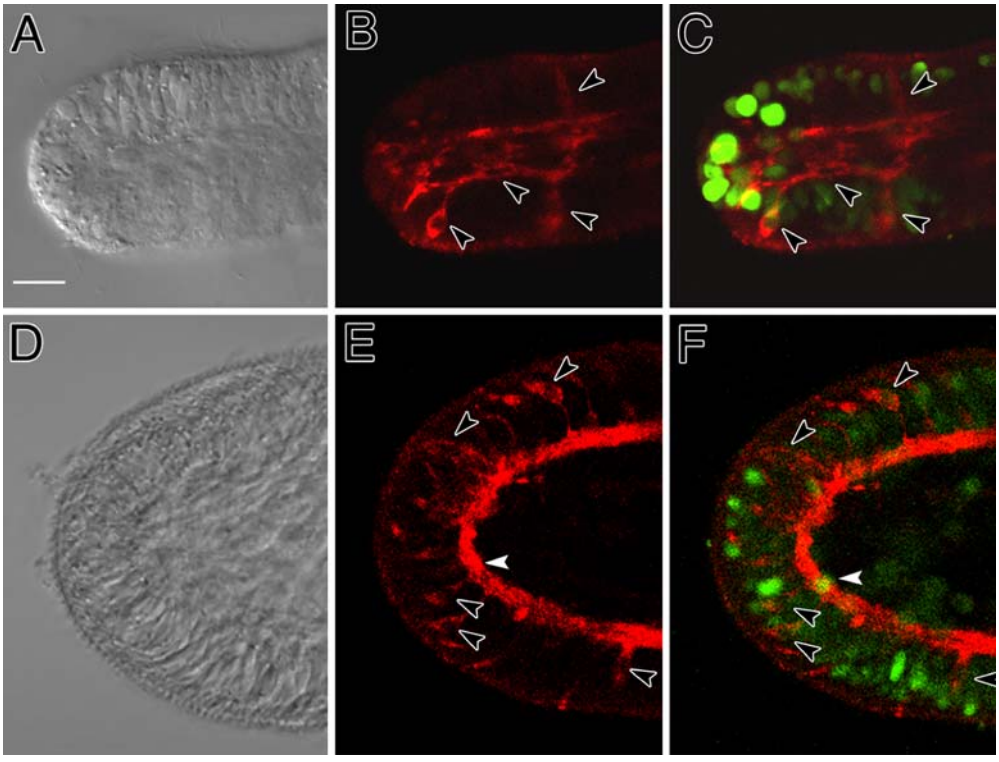

Fig. 9 Timing of apoptosis in nerve cells. Gln-ASW-treated larvae were double-stained with 1E11 monoclonal antibody and TUNEL reagent. Their arms are shown in brightfield (**a**, **d**) and darkfield (**b**, **c**, **e**, **f**) images (laser scanning microscopy). **a**–**c** At 0% resorption, no nerve cells (*red*) are seen to overlap with apoptotic cells (*green*). Note that the nuclei of nerve cells are TUNEL-negative (*black arrowheads*). **d**–**f** At 50% resorption, only one nucleus is TUNEL-positive (*white arrowhead*), whereas others are negative (*black arrowheads*). Nerve fibers are also seen to orient without disorder underneath the epithelia. *Bar* 10 μm

References

Araujo H, Machado LCH, Octacílio-Silva S, Mizutani CM, Silva MJF, Ramos RGP (2003) Requirement of the roughest gene for differentiation and time of death of interommatidial cells during pupal stages of *Drosophila* compound eye development. Mech Dev 120:537–547

Beer A-J, Moss C, Thorndyke M (2001) Development of serotonin-like and SALMFamide-like immunoreactivity in the nervous system of the sea urchin *Psammechinus miliaris*. Biol Bull 200:268–280

Berry DL, Schwartzman RA, Brown DD (1998) The expression pattern of thyroid hormone response genes in the tadpole tail identifies multiple resorption programs. Dev Biol 203:12–23

Biederbick A, Kern HF, Elsässer HP (1995) Monodansylcadaverine (MDC) is a specific in vivo marker for autophagic vacuoles. Eur J Cell Biol 66:3–14

Bowen ID, Morgan SM, Mullarkey K (1993) Cell death in the salivary glands of metamorphosing *Calliphora vomitoria*. Cell Biol Int 17:13–33

Burke RD (1983) Neural control of metamorphosis in *Dendraster excentricus*. Biol Bull 164:176–188

Cameron RA, Fraser S, Britten RJ, Davidson EH (1991) Macromere cell fates during sea urchin development. Development 113:1085–1091

Chia F-S, Burke RD (1978) Echinoderm metamorphosis: fate of larval structures. In: Chia F-S, Rice ME (eds) Settlement and metamorphosis of marine invertebrate larvae. Elsevier, New York, pp 219–234

Clarke PGH (1990) Developmental cell death: morphological diversity and multiple mechanisms. Anat Embryol 181:195–213

Dai J-D, Gilbert LI (1997) Programmed cell death of the prothoracic glands of *Manduca sexta* during pupal-adult metamorphosis. Insect Biochem Mol Biol 27:69–78

Dan-Sohkawa M, Suzuki J, Towa S, Kaneko H (1993) A comparative study on the fusogenic nature of echinoderm and nonechinoderm phagocytes in vitro. J Exp Zool 267:67–75

Das B, Schreiber AM, Huang H, Brown DD (2002) Multiple thyroid hormone-induced muscle growth and death programs during metamorphosis in *Xenopus laevis*. Proc Natl Acad Sci USA 99:12230–12235

Elinson RP, Remo B, Brown DD (1999) Novel structural elements identified during tail resorption in *Xenopus laevis* metamorphosis: lessons from tailed frogs. Dev Biol 215:243–252

Estabel J, Mercer A, Köning N, Exbrayat J-M (2003) Programmed cell death in *Xenopus laevis* spinal cord, tail and other tissues, prior to, and during, metamorphosis. Life Sci 73:3297–3306

Fox H (1973) Degeneration of the nerve cord in the tail of *Rana temporaria* during metamorphic climax: study by electron microscopy. J Embryol Exp Morphol 30:377–396

Hiesinger PR, Reiter C, Schau H, Fischbach K-F (1999) Neuropil pattern formation and regulation of cell adhesion molecules in *Drosophila* optic lobe development depend on synaptobrevin. J Neurosci 19:7548–7556

Ishizuya-Oka A (1996) Apoptosis of larval cells during amphibian metamorphosis. Microsc Res Tech 34:228–235

Kinch G, Hoffman KL, Rodrigues EM, Zee MC, Weeks JC (2003) Steroid-triggered programmed cell death of a motoneuron is autophagic and involves structural changes in mitochondria. J Comp Neurol 457:384–403

Menon J, Gardner EE, Vail S (2000) Developmental implications of differential effects of calcium in tail and body skin of anuran tadpoles. J Morphol 244:31–43

Metchnikoff E (1968) Lecture V. In: Lectures on the comparative pathology of inflammation. Dover, New York, pp 56–74

Nakajima Y, Kaneko H, Murray G, Burke RD (2004) Divergent patterns of neural development in larval echinoids and asteroids. Evol Dev 6:95–104

Papadimitriou JM, Walters MN (1979) Macrophage polykarya. CRC Crit Rev Toxicol 6:211–255

Pavans de Ceccatty M (1982) In vitro aggregation of syncytia and cells of a Hexactinellida sponge. Dev Comp Immunol 6:15–22

Sato Y (2003) Apoptosis of retracting larval tissues during metamorphosis of sea urchin. Hiyoshi Rev Nat Sci Keio University 35:19–27 (in Japanese)

Sato Y, Yazaki I (1999) A cellular analysis of sea urcin metamorphosis induced by L-glutamine. In: Carnevali MDC, Bonasoro F (eds) Echinoderm research 1998. Balkema, Rotterdam, pp 221–226

Schweichel JU, Merker HJ (1973) The morphology of various types of cell death in prenatal tissues. Teratology 7:253–266

Seipp S, Schmich J, Leitz T (2001) Apoptosis—a death-inducing mechanism tightly linked with morphogenesis in *Hydractina echinata* (Cnidaria, Hydrozoa). Development 128:4891–4898

Silva JRMC (2000) The onset of phagocytosis and identity in the embryo of *Lytechinus variegatus*. Dev Comp Immunol 24:733–739

Silva JRMCD (2002) Role of the phagocytes on embryos: some morphological aspects. Microsc Res Tech 57:498–506

Tamboline CR, Burke RD (1992) Secondary mesenchyme of the sea urchin embryo: ontogeny of blastocoelar cells. J Exp Zool 262:51–60

Tamura M, Dan-Sohkawa M, Kaneko H (1998) Coelomic pouch formation in reconstructing embryos of the starfish *Asterina pectinifera*. Dev Growth Differ 40:567–575

Taniguchi K, Kurata K, Maruzoi T, Suzuki M (1994) Dibromomethane, a chemical inducer of larval settlement and metamorphosis of the sea urchin *Strongylocentrotus nudus*. Fisheries Sci 60:795–796

Yazaki I (1995) Quantitative analysis of metamorphosis induced by L-glutamine in embryos of the sea urchin, *Hemicentrotus pulcherrimus*. Zool Sci 12:105–112

Yazaki I (2002) Mechanisms of sea urchin metamorphosis: stimuli and responses. In: Yokota Y, Matranga V, Smolenicka Z (eds) The sea urchin: from basic biology to aquaculture. Swets & Zeitlinger, Lisse, pp 51–71

Yazaki I, Harashima H (1994) Induction of metamorphosis in the sea urchin, *Pseudocentrotus depressus*, using L-glutamine. Zool Sci 11:253–260

Zakeri Z, Bursch W, Tenniswood M, Lockshin RA (1995) Cell death: programmed, apoptosis, necrosis, or other? Cell Death Differ 2:87–96